

Perceptual Deep Neural Networks: Adversarial Robustness through Input Recreation

Danilo Vasconcellos Vargas
Kyushu University, Japan
vargas@inf.kyushu-u.ac.jp

Bingli Liao
Kyushu University, Japan

Takahiro Kanzaki
Kyushu University, Japan

Abstract

Adversarial examples have shown that albeit highly accurate, models learned by machines, differently from humans, have many weaknesses. However, humans' perception is also fundamentally different from machines, because we do not see the signals which arrive at the retina but a rather complex recreation of them. In this paper, we explore how machines could recreate the input as well as investigate the benefits of such an augmented perception. In this regard, we propose Perceptual Deep Neural Networks (φ DNN) which also recreate their own input before further processing. The concept is formalized mathematically and two variations of it are developed (one based on inpainting the whole image and the other based on a noisy resized super resolution recreation). Experiments reveal that φ DNNs can reduce attacks' accuracy substantially, surpassing state-of-the-art defenses in 87% of the tests for adversarial training variations and 100% of the tests when only comparing with other pre-processing type of defenses. Moreover, the recreation process intentionally corrupts the input image. Interestingly, we show by ablation tests that corrupting the input is, although counter-intuitive, beneficial. This suggests that the blind-spot in vertebrates might also be, analogously, the precursor of visual robustness. Thus, φ DNNs reveal that input recreation has strong benefits for artificial neural networks similar to biological ones, shedding light into the importance of the blind-spot and starting an area of perception models for robust recognition in artificial intelligence.

1. Introduction

Recent work has revealed that albeit highly accurate, deep neural networks are far from robust [34]. The lack of robustness exist even for extremely small perturbations and simple transformations [23, 10, 33]. A wide range of defenses were proposed in recent years [12, 13, 21, 25, 22]. However, most of them have shortcomings such as relying on obfuscated gradients [1] or being biased by the type of perturbation used

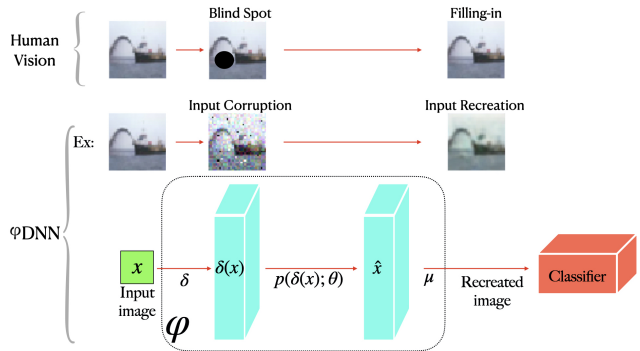


Figure 1: Illustration of the proposed φ DNN architecture and its similarity to the filling-in phenomena in human vision. Input x is initially corrupted by $\delta(x)$, removing some information while keeping contextual clues. One or multiple $p(\delta(x); \theta)$ uses this corrupted image to predict a partial reconstruction which is then aggregated with function μ and sent to the vanilla classifier.

to train (e.g., adversarial training) [19, 17].

Humans are less affected by small changes in the input. Interestingly, this is true even when part of the input is completely removed; which happens every second. Each of our eyes have a blind spot¹ where light cannot be perceived. Albeit this limitation, when we close one eye we do not see a black spot but a completely filled perception of an image [7, 18]. This is an example of how the brain is always predicting what it is viewing, revealing that biological perceptual systems are active rather than passive [24]. Thus, the images we see every second is rather a creation than mere signals that arrived in the brain, also called perception filling-in and related to predictive coding [5, 29, 9].

*Could deep neural networks also benefit
from actively creating its own input?*

To answer the question above we developed two percep-

¹The blind spot in each eye is where the optic nerve passes through the optic disc and therefore no photoreceptor cells are present.

tual systems that recreate the input image with predictions of it. One is based on inpainting all parts of the image (Section 3.2) while the other is based on recreating a super resolution of the image and then resizing it (Section 3.2). The recreated input is then fed to a deep neural network which has no access to the original input (Figure 1). Attacks on both systems suggest that by recreating the input robustness against adversarial attacks increase. Furthermore, the input recreation is not mutually exclusive with many of the previous defenses. It can be used together with adversarial training, for example, to improve further robustness.

Our contributions. In this paper, we present input recreation as a novel paradigm to enhance robustness against adversarial samples. The key contributions can be summarized as follows:

- We introduce deep neural networks (DNN) that create their own input based solely on contextual hints from the input, called perceptual DNNs (φ DNN). We describe φ DNNs formally and conduct experiments on two different implementations of it.
- We propose an inpainting based φ DNN. It works by predicting removed parts of the image and then joining the predicted parts together in a single completely recreated image. This recreated image is then used as input to a DNN.
- We propose a super resolution based φ DNN which recreates a higher resolution version of the input excluding at the same time any noise present in the original one. The image is later resized and inputted to a DNN.
- We conduct tests with white-box and black-box attacks to evaluate the robustness against adversarial samples. The results suggest that approaches with active perceptual systems recreating their own input can achieve higher robustness than their counterparts. This is true not only for the best performing system but most of its numerous variations, revealing a strength of the approach. Moreover, φ DNNs can be used jointly with other defenses for further increasing robustness.
- Results here suggests that the blind-spot in vertebrates might also, analogously, induce both robustness and a primitive form of imagination that recreates the input.

2. Related Works

Attack Methods. In this paper, we make use of attack methods for the sole purpose of evaluating the robustness of defenses and neural network models. Several attack models have been proposed in recent studies. They can be broadly categorized into white box [34, 12, 23, 3] and black box

attacks [26, 2, 16, 36, 8]. Many white box models can be summarized as follows. Given a target classifier C and a input pair (x, y) . Let \mathcal{L} be the adversarial loss for the classifier $C(x')$ e.g., the cross-entropy loss, and the ℓ_p norm used to measure the distance between the legitimate input x and the adversarial input x' . Generally, white box attack methods have been proposed by solving the constrained optimization problem:

$$\min_{x'} \mathcal{L}(C(x'), y), \quad \text{s.t.} \quad \|x - x'\|_p \leq \epsilon. \quad (1)$$

Examples of white box attacks are FGSM, one of the earliest white box attacks, which uses one-step approach to determine the direction to change the pixel value, [12] and an improved method called projected gradient descent (PGD) with a multiple-step variant [23]. In contrast, black box attacks have been proposed under more critical and practical conditions with the trade-offs of being slower. Here, we are also interested in black box attacks which are not based on estimating gradients and therefore can find adversarial samples even when the gradient is masked [1]. Therefore, tests with more straightforward black box attack methods based on evolutionary strategy such as the one-pixel attack and few-pixel attack fits the purpose [33].

Defenses to Adversarial Attacks. Recent studies have proposed various defense mechanisms against the threat of adversarial attacks. Albeit recent efforts, there is not yet a completely effective method. Defensive distillation, for example, proposed a smaller neural network which squeezed the content learned by the original one [27], however, it was shown to lack robustness in a later paper [3]. Adversarial training which was firstly proposed by Goodfellow *et al.* [12] increases the robustness by adding adversarial examples to the training set [15], [23]. Similarly, adversarial training was also shown vulnerable to attacks in [35]. Other defenses include pre-processing defenses such as the feature squeezing (FS) and spatial smoothing (SS) [40]. The objective here is to remove adversarial perturbation in a pre-processing stage. Recently there are a huge number of defenses proposed, however, they use mostly variations of gradient masking to avoid being attacked which do not confer greater security [1]. Regarding GAN based defenses, Defense-GAN [31] is based on training a generative adversarial network (GAN) to learn the distribution of original images. Each input would then be used to search for the closest projected input image learned by the generator before proceeding to classification. One of the main shortcomings is that the distribution learned by the generator is strictly limited by the training data set and the input image might be mapped into an illegitimate space. Albeit using GANs in our proposed approach, it shares no other similarities to Defense-GAN. Here, GANs predict parts of the input using the contextual information present and after the input has been severely corrupted by a simple function.

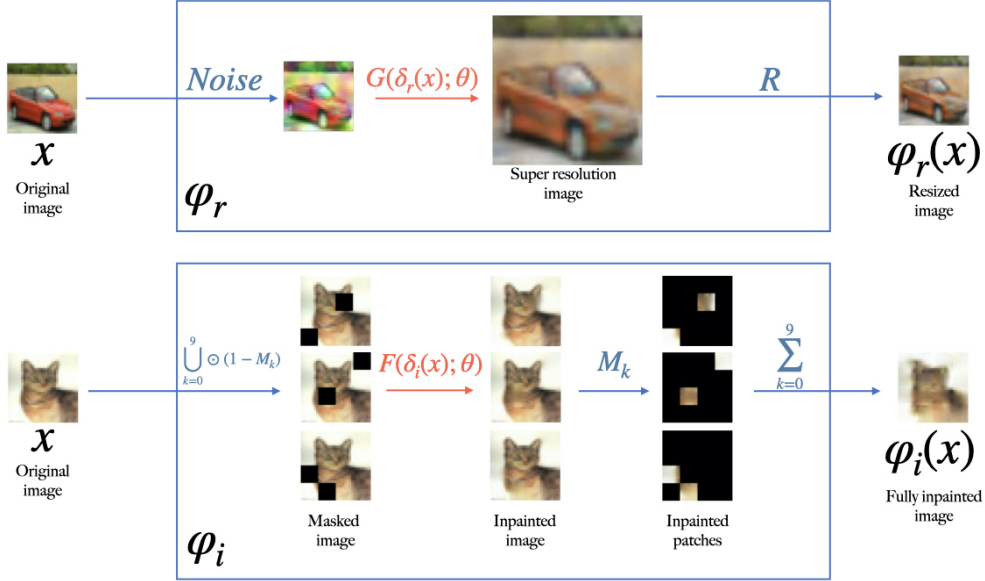


Figure 2: Illustration of the two implementations of φ DNNs proposed: Noisy Super-Resolution Reconstruction based (top) and Full Inpainting Reconstruction based (bottom).

Predictive Coding. Although φ DNNs do not necessarily use many of the components of predictive coding, it is loosely based on it. Predictive coding is a theory in neuroscience which demonstrates that the brain achieves high visual robustness by dynamically updating and predicting neural activities from the environment [28]. Previous studies have shown that the brain uses similar representations with CNNs, but CNNs are not as robust as the brain [4, 39]. Though there is still no perfect theoretical explanation for how it works, biological plausible models describe it as a recurrently connected hierarchical neural networks [32]. Recent research on predictive coding based CNNs imitating the feedforward, feedback, and recurrent connections performed well in object recognition [38].

This work makes use of both Generative Adversarial Network (GAN) and Variational AutoEncoder (VAE) to reconstruct the images. They are described briefly as follows.

2.1. Generative Adversarial Network

Generative Adversarial Network (GAN) is a powerful generative model that consists of two neural networks: a generator network which learns the probability distribution of the input and a binary discriminator network which distinguishes between generated data and the input data. Goodfellow *et al.* [11] originally introduced a GAN to solve the following min-max loss function:

$$\min_G \max_D \mathbb{E}_{x \sim p_{data}(x)} [\log D(x)] + \mathbb{E}_{z \sim p_z(z)} [\log(1 - D(G(z)))]. \quad (2)$$

where p_{data}, p_z represent the data distribution from the input and the generator, \max_D maximizes the difference between p_{data} and p_z , while \min_G converges to minimum when p_{data} equals p_z .

Super-resolution GAN (SRGAN). Super-resolution GAN (SRGAN) generates a photo-realistic high-resolution (HR) image from its downsampled low-resolution (LR) input image [20]. They used VGG-19 network to extract high dimension features and designed an alternative function, the perceptual loss function which consists of content loss and adversarial loss, to solve the following optimization problem:

$$\min_G \max_D \mathbb{E}_{I^{HR} \sim p_{train}(I^{HR})} [\log D(I^{HR})] + \mathbb{E}_{I^{LR} \sim P_G(I^{LR})} [\log(1 - D(G(I^{LR})))]]. \quad (3)$$

Here, the generative model G maps a given LR input I^{LR} to its HR counterpart I^{HR} . The discriminator D is trained to distinguish between the produced I^{HR} images from real inputs.

2.2. Autoencoder based Inpainting

Inpainting is defined as the synthesis of content to fill missing image parts. Here, we use an Autoencoder (AE) to predict the missing pixels with a simple UNET-like architecture [37, 30]. Let a masked image x_0 be represented as $x_0 = x \odot (1 - M)$, in which M is a binary mask, x is the original input image and \odot is the element-wise product

operation. Inpainting can be formulated as the following energy minimization problem:

$$\begin{aligned} \min_{\theta} E(F(x_0; \theta); x), \\ E(F(x_0; \theta); x) = |(F(x_0; \theta) - x)|, \end{aligned}$$

where F is the resulting function from the AE with parameters θ .

3. φ DNNs

In this section, we describe formally the φ DNN architecture, its motivation as well as two different implementations of it.

3.1. The Technical Motivation Behind Input Recreation

Beyond the bio-inspired aspect, there are some technical importance for recreating the input in a similar way to humans and other animals. First, by recreating the input, the neural network and not the environment defines which input will be responsible for the output of the system. This type of actively modified input provides further control of the input to avoid contextual problems or other issues beyond adversarial samples. Second, it is now possible to constrain the probability distribution of the input further. This can be done in many ways and is only slightly explored here with added noise. Third, with perceptual changes happening all the time, attacking becomes a time-varying function which might be impossible to repeat. This would make calculated attacks near impossible. Fourth, when facing φ DNNs, the attacker has less information about the network for he/she does not know even the input now. Lastly, gradient-based and gradient estimation based approaches tend to perform poorly if the input recreation is well designed.

3.2. φ DNN's Architecture

Consider the perceptual tuple φ and its respective function $\varphi(x)$ as follows:

$$\varphi := \langle \delta, p(\delta(x); \theta), \mu \rangle, \quad (4)$$

$$\varphi(x) = \mu(p(\delta(x); \theta)), \quad (5)$$

where δ is a function that corrupts the input, removing some information from it and returning one or multiple images; $p(\delta(x); \theta)$ is the probability distribution learned by the perceptual layer that predicts x from the corrupted input $\delta(x)$ based on its learned weights θ ; and μ is the aggregation function which corrects the output from the perceptual layer to be the same as original input x .

φ DNN is defined as follows:

$$\varphi\text{DNN} := C(\varphi(x)), \quad (6)$$

in which C is a classifier that receives as input the output from the perceptual function $\varphi(x)$.

Noisy Super-Resolution Reconstruction (NSR) Here we define an implementation of the φ DNN's architecture using super resolution and images corrupted with noise. Note that images are always corrupted with noise. Let x be a given input and R a function which resizes the high resolution image to the original resolution. The process can be defined as follows:

$$\varphi_r = \langle \delta_r, p_r(\delta(x); \theta_r), \mu_r \rangle, \quad (7)$$

$$\text{where } \delta_r = \text{Noise}, p_r = G(\delta(x); \theta), \mu_r = R.$$

note that Noise is an arbitrary noise function which returns a noisy image. $G(\delta(x); \theta)$ is the generator of SRGAN which maps an image from low resolution to high resolution and tries to clean the always present noise (illustrated in Figure 2).

Full Inpainting Reconstruction (FIR) To demonstrate that φ DNNs can be developed in many forms, here, we propose a φ DNN based on inpainting the whole image. Specifically, φ_i is defined as follows.

$$\varphi_i = \langle \delta_i, p_i(\delta(x); \theta_i), \mu_i \rangle, \quad (8)$$

$$\text{where } \delta_i(x) = \bigcup_{k=0}^9 \odot(1 - M_k) \cdot x,$$

$$p_i = F(\delta(x); \theta), \mu_i(x) = \sum_{k=0}^9 M_k \cdot x,$$

where M_k are masks such that their sum is equal to the identity matrix ($\sum_{k=0}^9 M_k = I$) and their multiplication is equal to 0 ($\prod_{k=0}^9 M_k = 0$). Therefore, each of the masks hide a specific part of the image and together they mask the whole image. $\delta_i(x)$ (i.e., $\bigcup_{k=0}^9 \odot(1 - M_k) \cdot x$) creates a set with 10 masked inputs. All masked inputs are then inpainted with $F(\delta(x)); \theta$ and lastly all inpainted parts are joined together through $\sum_{k=0}^9 M_k \cdot x$. Figure 2 shows an illustration of the process.

4. Experiments

To evaluate φ DNN architecture, we test here the robustness of two implementations of it (i.e., FIR and NSR) by attacking them with different types of attacks. The proposed architecture is also compared with other defenses and we explore the possibility of employing it together with other defenses.

Settings. To evaluate the robustness of systems avoiding biases and the sole presence of gradient masking, we employ two white box attacks (FGSM and PGD) as well as non-gradient based black box attacks (one pixel and ten pixel attack). In this paper, every attack is repeated for 500 random

Table 1: Comparison between Feature Scattering (the current state-of-the-art defense) and the two proposed φ DNNs with adversarial training on CIFAR10 (NSR_{adv} and FIR_{adv}). Results show the attack accuracy over the defenses. For reference, φ DNNs without adversarial training (NSR and FIR), only ResNet with the same adversarial training used on NSR_{adv} and FIR_{adv} (ResNet_{adv}) and vanilla ResNet are also included.

Defense	test acc	1px attack	10px attack	FGSM ($\epsilon = 8$)	PGD ($\epsilon = 8$)
Ours: NSR _{adv}	0.827	0.074	0.086	0.089	0.087
Ours: FIR _{adv}	0.885	0.028	0.038	0.046	0.126
FScattering	0.900	0.041	0.586	0.128	0.237
NSR	0.838	0.092	0.107	0.244	0.173
FIR	0.894	0.042	0.044	0.714	0.944
ResNet _{adv}	0.892	0.200	0.838	0.718	1.000
ResNet	0.930	0.308	0.962	0.810	1.000

Table 2: Comparison between Feature Scattering (the current state-of-the-art defense) and the two proposed φ DNNs with adversarial training on SVHN (NSR_{adv} and FIR_{adv}). Results show the attack accuracy over the defenses. For reference, φ DNNs without adversarial training (NSR and FIR), only ResNet with the same adversarial training used on NSR_{adv} and FIR_{adv} (ResNet_{adv}) are also included.

Defense	test acc	1px attack	10px attack	FGSM ($\epsilon = 8$)	PGD ($\epsilon = 8$)
Ours: NSR _{adv}	0.924	0.011	0.041	0.080	0.060
Ours: FIR _{adv}	0.930	0.004	0.004	0.000	0.012
FScattering	0.962	0.000	0.010	0.132	0.459
NSR	0.930	0.026	0.066	0.200	0.080
FIR	0.964	0.014	0.040	0.492	0.918

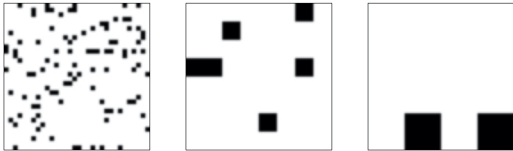


Figure 3: Three masks created for FIR with grid size of respectively (from left to right) 1, 4 and 8.

images of the test data set with the average attack accuracy being reported. AllConv neural network is the main neural network used for both FIR and NSR, although some tests with different models are present. For all experiments, the CIFAR-10 dataset is normalized to the range $[0, 1]$. The machines used in the experiments are equipped with NVIDIA GeForce RTX 2080 Ti and AMD Ryzen 9 3950x 16-core. The deep neural networks used by our proposed methods after the $\varphi(x)$ transformation are not augmented.

Regarding FIR, 10 masks are created, each of them removing 10% of the image (Figure 3). To create the masks, a grid of a given size is set over the 32×32 image and then multiple pieces of this grid are randomly selected to form

one mask. Pieces are selected until 10% of the image is covered. The inpainting model is trained with a corresponding mask size covering 10% of the image and with epochs and batch size of respectively 20 and 32.

Regarding NSR, to create the training dataset for SRGAN we resize CIFAR-10 dataset to 128×128 as the high resolution ground truth and add noise to the training dataset during training. The type of noise used is bi-linear interpolation for both up and downsizing. In order to match with the normalization, we replace tanh with sigmoid as the activation function for the last convolution layer in SRGAN’s generator. We train SRGAN with 1000 epochs and set batch size to 20 to ensure convergence.

4.1. Comparison with other Defenses

Tables 1 and 2 compare the last development in adversarial training, i.e. Feature Scattering [41], with the proposed algorithms and variations of them trained with a simple adversarial training. Results show that φ DNNs with adversarial training surpass FScattering for most (7 out of the 8 experiments) of the widely different attacks tested. It is known that adversarial training methods such as FScattering perform

Table 3: Comparison of proposed methods with other pre-processing based defenses. NSR and FIR models use the best setting from Tables 4 and 5 while the other ones use AllConv and the best settings out of a couple of experiments.

Defense	test acc	1px attack	10px attack	FGSM ($\epsilon = 8$)	PGD ($\epsilon = 8$)
Ours: NSR	0.838	0.092	0.107	0.244	0.173
Ours: FIR	0.894	0.042	0.044	0.714	0.944
FS	0.792	0.468	0.978	0.782	1.000
SS	0.786	0.132	0.522	0.744	0.988
JPEG	0.730	0.662	0.996	0.568	0.926
LS	0.914	0.370	0.954	0.448	1.000

Table 4: Attack accuracy for both NSR and SR (NSR without the added noise $\delta_r(\cdot)$) trained with different types of noise and connected to ResNet. We tested Gaussian noise with 0 mean (μ), and variances (σ^2) of 0.01. For Panda noise, the scalar number (0.01) represents the probability (α and β) of white and black pixels present in the image. $A + B$ represents that two types of noises A and B are summed together. The subscript T means that the classifier was retrained with a data set made of reconstructed images (i.e., images from $\varphi_r(x)$).

Defense	Noise	test acc	10px attack	FGSM ($\epsilon = 8$)	PGD ($\epsilon = 8$)
NSR	+ResNet[Guassain0.01]	0.792	0.404	0.186	0.140
SR	+ResNet[Guassain0.01]	0.774	0.928	0.206	0.110
NSR	+ResNet[Panda0.01]	0.910	0.290	0.222	0.262
SR	+ResNet[Panda0.01]	0.915	0.212	0.724	0.880
NSR	+ResNet[Guassain+Panda]	0.770	0.122	0.184	0.134
SR	+ResNet[Guassain+Panda]	0.819	0.348	0.250	0.138
NSR	+ResNet[Guassain+Panda] _T	0.838	0.107	0.244	0.173
SR	+ResNet[Guassain+Panda] _T	0.805	0.836	0.220	0.136

poorly when the attacking distribution differ from the data used to learn. This applies to FScattering as well which can be attacked with nearly 60% with 10px attack. Having said that, it is impressive that both NSR and FIR can surpass FScattering even on FGSM and PGD which are close to the augmented distribution of noisy images it used to learn. Notice that the same adversarial training that has little change on the vanilla Resnet (i.e., ResNet_{adv}) is very effective on NSR and FIR. For example, PGD attack accuracy on FIR_{adv} is 86% lower than vanilla FIR. Thus, it is expected that if a state-of-the-art adversarial training is applied to NSR and FIR, their robustness should improve even further.

In fact, if we take into account that FScattering and φ DNN are (a) different in nature and (b) can be also used together. It can be justified that φ DNNs should be compared with other pre-processing defenses and not adversarial training ones. We follow this rational and compare the proposed methodology in Table 3 with other pre-processing defenses such as FS, SS, JPEG compression defence (JPEG) [6] and Label Smoothing (LS) [14]. Here all defenses and FIR used AllConv and NSR used ResNet as the classifier. Note that

we also tried to include DefenseGAN but it failed to learn properly on CIFAR10.

Both φ DNNs surpass all others in all attacks for Table 3. The result is expected since φ DNNs do not only pre-process images, they recreate them based on contextual information and previous learned distribution.

4.2. NSR Analysis: When Losing Information is Beneficial

NSR corrupts the input image possibly losing some information. Here we will investigate if this loss of information has any deleterious consequences. We will also analyze the behavior of NSR on adversarial samples.

To analyze the influence of the initial input corruption by $\delta_r(x)$, an ablation test is made, in which $\delta_r(x)$ is removed from $\varphi_r(x)$ (SR in Table 4).

Results show an increased robustness and similar accuracy. Specifically, in 8 out of 12 tests, the robustness of NSR surpassed the ablated algorithm SR. Regarding the accuracy, both NSR and SR performed similarly. NSR surpassed it in half the tests and was surpassed in the other half.

Table 5: Comparing the difference of grid size on FIR’s accuracy and robustness. ResNet is the vanilla classifier while FIR_1^+ , FIR_4^+ and FIR_8^+ means using ResNet in the FIR’s architecture with grid size of respectively 1, 4 and 8. Each inpainting model is trained with the corresponding grid size only, and the classifier model is trained with corresponding inpainting image from $\varphi_i(x)$.

	Test accuracy	1px attack	10px attack	FGSM ($\epsilon = 8$)	PGD ($\epsilon = 8$)
ResNet	0.930	0.308	0.962	0.810	1.000
FIR_1	0.894	0.042	0.044	0.714	0.944
FIR_4	0.828	0.212	0.592	0.448	0.396
FIR_8	0.749	0.298	0.656	0.370	0.276

These results reveal, perhaps counter-intuitively, that always adding noise ($\delta_r(x)$) to the input is mostly beneficial for neural networks that reconstruct their input. On average, it usually improves robustness while leaving accuracy unchanged. There are two reasons for such a behavior: (a) always adding noise constrains the image distribution to non-smooth pixel transitions and (b) an always changing input is harder to attack.

Figure 4 shows a sample behavior of φ_r . $\delta_r(x)$ corrupts strongly x but SRGAN is able to recover most of it, resulting in a clean $\varphi_r(x)$ image. Similar behavior happens to adversarial sample x' . The difference between $\varphi_r(x)$ and $\varphi_r(x')$ is substantially small and diluted compared to x and x' which reveals that φ_r worked well despite the negative result.

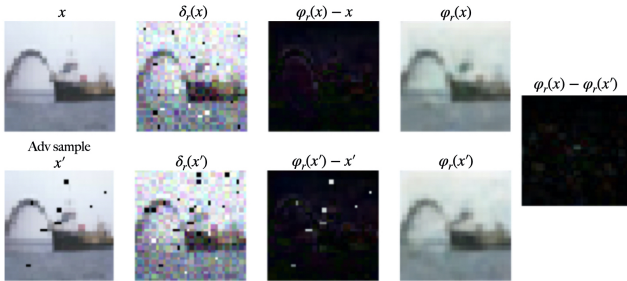


Figure 4: Behavior of an image sample x and its respective adversarial sample x' throughout $\varphi_r(x)$.

4.3. FIR Analysis

In this section, FIR will be analyzed with relation to its grid size, as well as its behavior for adversarial and original samples. For L0 attacks (1px, 5px and 10px attacks), FIR performs better with lower grid values while higher grid values are better suited to L_∞ attacks (PGD and FGSM) (Table 5). This is expected since L0 attacks perturbs fewer pixels and therefore punctual corrections are better. The opposite is true for L_∞ . Figure 5 reveals that inpainting is still limited in accuracy and therefore grids greater than one

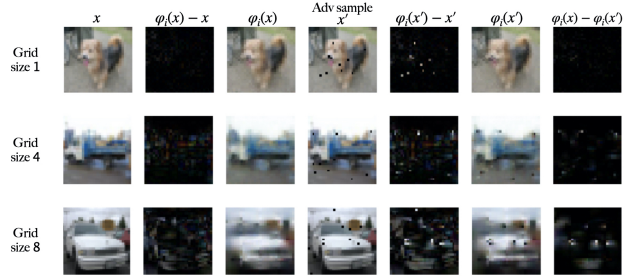


Figure 5: Behavior of $\varphi_i(x)$ on an image sample x and its respective adversarial sample x' .

have lower quality. Furthermore, an attack that modifies one pixel at the border of a mask, might cause an even stronger perturbation if the inpainting method uses that attacked pixel as contextual information. This happened in Figure 5 for the $\varphi_i(x')$ with the car and demonstrates the weakness of bigger grids (or perhaps of current inpainting algorithms). Attacking FIR is difficult because for a pixel to be modified in the final image $\varphi_i(x)$, many pixels around it must be changed, in the case of lower grid values, or pixels near the mask needs to be changed, in the case of higher grid values. This creates a bigger burden on the attacker and causes many attacks to fail. A simple version of adversarial training (with FGSM created adversarial samples) improves substantially the advantages of FIR, allowing it to even surpass the state-of-the-art (Table 1).

5. Blind-spot as a Robustness Feature

Results with input reconstructing neural networks (φ DNNs) revealed intriguing benefits of the $\delta(x)$ (i.e., of removing parts or corrupting the input). In vertebrates, blind-spot and the filling-in phenomena are analogous to respectively the $\delta(x)$ and the input reconstruction process. Thus, the results here suggest that blind-spot might improve robustness. It may also incentive, throughout evolution, in the development of filling-in (input reconstruction), because recreation of the input becomes a necessity. Moreover, once

filling-in is existent, it is expected that the blind-spot becomes mostly beneficial.

6. Conclusions

In this paper, we proposed perceptual deep learning networks which make use of corrupting functions and context-based prediction and aggregation to reconstruct the input. We showed that, perhaps surprisingly, corrupting the input is beneficial to robustness. Moreover, similar to biological neural networks, the input reconstruction, albeit different from its initial one, has many advantages which includes more control, constrained probabilities and unpredictability from attacker’s perspective (i.e., now the attacker does not know even the input).

Current results suggest that the proposed architecture is robust to all types of attacks (e.g., no bias to L_0 or L_∞ was spotted), surpassing the state-of-the-art in adversarial training and many other pre-processing based defenses. Having said that, our exploration of the architecture was non-exhaustive. We introduced only two implementations of the φ DNN’s architecture. There are certainly many more powerful and interesting variations.

Last but not least, we conjecture that φ DNNs use a primitive type of imagination which can be further enhanced by not only improving GANs but by researching deeply into the question regarding its foundation, i.e., what defines a coherent perception?

Acknowledgment

This work was supported by JST, ACT-I Grant Number JP-50243 and JSPS KAKENHI Grant Number JP20241216.

References

- [1] Anish Athalye, Nicholas Carlini, and David Wagner. Obfuscated gradients give a false sense of security: Circumventing defenses to adversarial examples. In *Proceedings of the 35th International Conference on Machine Learning, ICML 2018*, July 2018.
- [2] W. Brendel, J. Rauber, and M. Bethge. Decision-based adversarial attacks: Reliable attacks against black-box machine learning models. In *International Conference on Learning Representations*, 2018.
- [3] Nicholas Carlini and David Wagner. Towards evaluating the robustness of neural networks. In *2017 IEEE Symposium on Security and Privacy (SP)*, pages 39–57. IEEE, 2017.
- [4] Radoslaw Martin Cichy, Aditya Khosla, Dimitrios Pantazis, Antonio Torralba, and Aude Oliva. Comparison of deep neural networks to spatio-temporal cortical dynamics of human visual object recognition reveals hierarchical correspondence. *Scientific reports*, 6:27755, 2016.
- [5] Andy Clark. Whatever next? predictive brains, situated agents, and the future of cognitive science. *Behavioral and brain sciences*, 36(3):181–204, 2013.
- [6] Nilaksh Das, Madhuri Shanbhogue, Shang-Tse Chen, Fred Hohman, Li Chen, Michael E Kounavis, and Duen Horng Chau. Keeping the bad guys out: Protecting and vaccinating deep learning with jpeg compression. *arXiv preprint arXiv:1705.02900*, 2017.
- [7] Peter De Weerd, Ricardo Gattass, Robert Desimone, and Leslie G Ungerleider. Responses of cells in monkey visual cortex during perceptual filling-in of an artificial scotoma. *Nature*, 377(6551):731–734, 1995.
- [8] Yinpeng Dong, Hang Su, Baoyuan Wu, Zhifeng Li, Wei Liu, Tong Zhang, and Jun Zhu. Efficient decision-based black-box adversarial attacks on face recognition. In *Proceedings of the IEEE Conference on Computer Vision and Pattern Recognition*, pages 7714–7722, 2019.
- [9] Benedikt V Ehinger, Katja Häusser, Jose P Ossandon, and Peter König. Humans treat unreliable filled-in percepts as more real than veridical ones. *Elife*, 6:e21761, 2017.
- [10] Logan Engstrom, Dimitris Tsipras, Ludwig Schmidt, and Aleksander Madry. A rotation and a translation suffice: Fooling cnns with simple transformations. *ArXiv*, abs/1712.02779, 2017.
- [11] Ian Goodfellow, Jean Pouget-Abadie, Mehdi Mirza, Bing Xu, David Warde-Farley, Sherjil Ozair, Aaron Courville, and Yoshua Bengio. Generative adversarial nets. In *Advances in neural information processing systems*, pages 2672–2680, 2014.
- [12] Ian Goodfellow, Jonathon Shlens, and Christian Szegedy. Explaining and harnessing adversarial examples. In *International Conference on Learning Representations*, 2015.
- [13] Kathrin Grosse, Praveen Manoharan, Nicolas Papernot, Michael Backes, and Patrick McDaniel. On the (statistical) detection of adversarial examples. *arXiv preprint arXiv:1702.06280*, 2017.
- [14] Tamir Hazan, George Papandreou, and Daniel Tarlow. *Perturbations, Optimization, and Statistics*. MIT Press, 2016.

- [15] Ruitong Huang, Bing Xu, Dale Schuurmans, and Csaba Szepesvári. Learning with a strong adversary. *arXiv preprint arXiv:1511.03034*, 2015.
- [16] Andrew Ilyas, Logan Engstrom, Anish Athalye, and Jessy Lin. Black-box adversarial attacks with limited queries and information. In *Proceedings of the 35th International Conference on Machine Learning, ICLR 2018*, July 2018.
- [17] Harini Kannan, Alexey Kurakin, and Ian J. Goodfellow. Adversarial logit pairing. *ArXiv*, abs/1803.06373, 2018.
- [18] Hidehiko Komatsu. The neural mechanisms of perceptual filling-in. *Nature reviews neuroscience*, 7(3):220–231, 2006.
- [19] Alexey Kurakin, J. Ian Goodfellow, and Samy Bengio. Adversarial machine learning at scale. *international conference on learning representations*, 2017.
- [20] Christian Ledig, Lucas Theis, Ferenc Huszár, Jose Caballero, Andrew Cunningham, Alejandro Acosta, Andrew Aitken, Alykhan Tejani, Johannes Totz, Zehan Wang, et al. Photo-realistic single image super-resolution using a generative adversarial network. In *Proceedings of the IEEE conference on computer vision and pattern recognition*, pages 4681–4690, 2017.
- [21] Xin Li and Fuxin Li. Adversarial examples detection in deep networks with convolutional filter statistics. In *Proceedings of the IEEE International Conference on Computer Vision*, pages 5764–5772, 2017.
- [22] Xingjun Ma, Bo Li, Yisen Wang, Sarah M Erfani, Sudanthi Wijewickrema, Grant Schoenebeck, Dawn Song, Michael E Houle, and James Bailey. Characterizing adversarial subspaces using local intrinsic dimensionality. In *6th International Conference on Learning Representations, ICLR 2018*, 2018.
- [23] Aleksander Madry, Aleksandar Makelov, Ludwig Schmidt, Dimitris Tsipras, and Adrian Vladu. Towards deep learning models resistant to adversarial attacks. In *International Conference on Learning Representations*, 2018.
- [24] James L McClelland and David E Rumelhart. An interactive activation model of context effects in letter perception: I. an account of basic findings. *Psychological review*, 88(5):375, 1981.
- [25] Jan Hendrik Metzen, Tim Genewein, Volker Fischer, and Bastian Bischoff. On detecting adversarial perturbations. In *Proceedings of 5th International Conference on Learning Representations (ICLR)*, 2017.
- [26] Nicolas Papernot, Patrick McDaniel, Ian Goodfellow, Somesh Jha, Z Berkay Celik, and Ananthram Swami. Practical black-box attacks against machine learning. In *Proceedings of the 2017 ACM on Asia conference on computer and communications security*, pages 506–519, 2017.
- [27] Nicolas Papernot, Patrick McDaniel, Xi Wu, Somesh Jha, and Ananthram Swami. Distillation as a defense to adversarial perturbations against deep neural networks. In *2016 IEEE Symposium on Security and Privacy (SP)*, pages 582–597. IEEE, 2016.
- [28] Cyriel MA Pennartz. *The brain’s representational power: on consciousness and the integration of modalities*. MIT Press, 2015.
- [29] Rajesh PN Rao and Dana H Ballard. Predictive coding in the visual cortex: a functional interpretation of some extra-classical receptive-field effects. *Nature neuroscience*, 2(1):79–87, 1999.
- [30] Olaf Ronneberger, Philipp Fischer, and Thomas Brox. U-net: Convolutional networks for biomedical image segmentation. In *International Conference on Medical image computing and computer-assisted intervention*, pages 234–241. Springer, 2015.
- [31] Pouya Samangouei, Maya Kabkab, and Rama Chellappa. Defense-GAN: Protecting classifiers against adversarial attacks using generative models. In *International Conference on Learning Representations*, 2018.
- [32] Olaf Sporns and Jonathan D Zwi. The small world of the cerebral cortex. *Neuroinformatics*, 2(2):145–162, 2004.
- [33] Jiawei Su, Danilo Vasconcellos Vargas, and Kouichi Sakurai. One pixel attack for fooling deep neural networks. *IEEE Transactions on Evolutionary Computation*, 23(5):828–841, 2019.
- [34] Christian Szegedy, Wojciech Zaremba, Ilya Sutskever, Joan Bruna, Dumitru Erhan, Ian Goodfellow, and Rob Fergus. Intriguing properties of neural networks. In *International Conference on Learning Representations*, 2014.
- [35] Florian Tramèr, Alexey Kurakin, Nicolas Papernot, Ian Goodfellow, Dan Boneh, and Patrick Drew McDaniel. Ensemble adversarial training: Attacks and defenses. In *6th International Conference on Learning Representations, ICLR 2018*, 2018.
- [36] Chun-Chen Tu, Paishun Ting, Pin-Yu Chen, Sijia Liu, Huan Zhang, Jinfeng Yi, Cho-Jui Hsieh, and Shin-Ming Cheng. Autozoom: Autoencoder-based zeroth

order optimization method for attacking black-box neural networks. In *Proceedings of the AAAI Conference on Artificial Intelligence*, volume 33, pages 742–749, 2019.

- [37] Dmitry Ulyanov, Andrea Vedaldi, and Victor Lempitsky. Deep image prior. In *Proceedings of the IEEE Conference on Computer Vision and Pattern Recognition*, pages 9446–9454, 2018.
- [38] Haiguang Wen, Kuan Han, Junxing Shi, Yizhen Zhang, Eugenio Culurciello, and Zhongming Liu. Deep predictive coding network for object recognition. In Jennifer Dy and Andreas Krause, editors, *Proceedings of the 35th International Conference on Machine Learning*, volume 80 of *Proceedings of Machine Learning Research*, pages 5266–5275, Stockholmmsässan, Stockholm Sweden, 10–15 Jul 2018. PMLR.
- [39] Haiguang Wen, Junxing Shi, Yizhen Zhang, Kun-Han Lu, Jiayue Cao, and Zhongming Liu. Neural encoding and decoding with deep learning for dynamic natural vision. *Cerebral Cortex*, 28(12):4136–4160, 2018.
- [40] Weilin Xu, David Evans, and Yanjun Qi. Feature squeezing: Detecting adversarial examples in deep neural networks. *arXiv preprint arXiv:1704.01155*, 2017.
- [41] Haichao Zhang and Jianyu Wang. Defense against adversarial attacks using feature scattering-based adversarial training. In *Advances in Neural Information Processing Systems*, 2019.

SUPPLEMENTARY WORK

This supplementary work includes noise descriptions, additional experiments on other datasets and parameters; and further examples of adversarial examples for φ DNNs.

G. NOISE DESCRIPTION

Panda noise. Given a pixel $\mathbf{g} = (R, G, B)$ in a RGB image \mathbf{I} , Panda noise can be defined as follows:

$$f(\mathbf{g}) = \begin{cases} \mathbf{g}, & P = 1 - (\alpha + \beta) \\ (255, 255, 255), & P = \alpha \\ (0, 0, 0), & P = \beta \end{cases}$$

where α and β are probabilities that a pixel in image \mathbf{I} will become respectively white or black.

ColorDepth noise. A RGB image represents feature information by color bit depths. For example, CIFAR-10 encodes images with 24-bit color depths. The ColorDepth noise reduces original images to fewer bits representation. Given a normalized RGB image \mathbf{I} that ranges from 0 to 1, and the target t-bits color depths after reducing, this noise could be formulated as:

$$\mathbf{I}' = \frac{[\mathbf{I} \cdot (2^t - 1)]}{2^t - 1}$$

where $[\]$ denotes the standard rounding function and \mathbf{I}' is the image encoded with t-bits color depths.

Gaussian noise. Given a RGB image \mathbf{I} , the Gaussian noise could be described as the following:

$$\mathbf{I}' = \mathbf{I} + R \sim \mathcal{N}(\mu, \sigma^2)$$

where R is the Gaussian filter.

H. ADDITIONAL EXPERIMENTS

NSR and FIR performance remains mostly the same in the SVHN dataset. Table 6 shows that even without adversarial training the reconstruction of the input already possess inherent robustness, similar to the results in CIFAR10.

Results in Table 7 reveals that NSR’s SRGAN trained with Panda noise performs better on both black and white box attacks when compared with it trained with Gaussian noise. Moreover, the robustness is further improved when we trained NSR with noise images consisting of half Panda noise and half ColorDepth noise. This is expected since the input image while testing always has the presence of noise, i.e., the probability of input from both training and testing gets closer to each other.

The results from table 8 demonstrate that there is no significant improvement when NSR is combined with other pre-processing methods such as FS and SS.

Table 6: Attack accuracy for the two proposed φ DNNs on SVHN.

Defense	test acc	1px attack	10px attack	FGSM ($\epsilon = 8$)	PGD ($\epsilon = 8$)
NSR	0.930	0.026	0.066	0.200	0.080
FIR	0.964	0.014	0.018	0.492	0.918

Table 7: Effect of different noise types on the δ_r of NSR. The symbol 1/2 means that half of the training images had a certain noise or clean images.

Noises	1px attack	10px attack	FGSM ($\epsilon=2.55$)	PGD ($\epsilon=2.55$)
NSR[1/2Gaussian+1/2Clean]	0.192	0.668	0.534	0.578
NSR[1/2Panda+1/2Clean]	0.080	0.256	0.446	0.428
NSR[1/2Panda+1/2ColorDepth]	0.058	0.182	0.292	0.286

I. TRAINING STRATEGY

We use Adam with learning scheduler in all experiments. Due to the poor performance of Adam in the adversarial training, the SGD with learning scheduler is used during the adversarial training. To improve neural network performance, we use learning scheduler to adjust learning rate. For Adam learning scheduler, the learning rate starts from 10^{-3} and increases to 10^{-1} then decreases to 10^{-2} , 10^{-3} and $0.5 * 10^{-3}$. For SGD learning scheduler, the learning rate starts from 10^{-1} and decreases to 10^{-2} and 10^{-3} . To match data normalization, we apply sigmoid activation function instead of tanh as the last layer output for generator model in SRGAN.

J. EXAMPLES OF IMAGES PROCESSED BY φ DNNs

Figure 6 to 9 contain some samples and the images from each stage of the φ_r DNN when processing these samples. Figure 10 follows a similar pattern but for φ_i DNN.

Table 8: Comparison of the resulting attack accuracy for NSR with and without other pre-processing defenses.

Defenses	1px attack	10px attack	FGSM ($\epsilon=2.55$)	PGD ($\epsilon=2.55$)
NSR	0.072	0.158	0.178	0.210
NSR+FS	0.190	0.208	0.212	0.204
NSR+SS	0.160	0.204	0.320	0.274

Table 9: Attack accuracy for both NSR and SR (NSR without the added noise $\delta_r(\cdot)$) trained with different types of noise and connected to AllConv and ResNet. We tested Gaussian noise with 0 mean (μ), and variances (σ^2) of 0.01 and 0.001. For Panda noise, the scalar number (0.01 and 0.05) represents the probability (α and β) of white and black pixels present in the image. For ColorDepth noise, the scalar number 3 represents reduction of image color-bit to 3 bits. $A + B$ represents that two types of noises A and B are summed together while the $A | B$ means it randomly generate either A or B with 50% probability each. The subscript T means that the classifier was retrained with a data set made of reconstructed images (i.e., images from $\varphi_r(x)$).

Type	Defense	test acc	1px attack	10px attack	FGSM ($\epsilon = 8$)	PGD ($\epsilon = 8$)
NSR	ResNet	0.930	0.308	0.962	0.810	1.000
	ResNet[Guassian0.01]	0.792	0.136	0.404	0.186	0.140
	ResNet[Guassian0.001]	0.892	0.218	0.670	0.554	0.456
	ResNet[Panda0.01]	0.910	0.174	0.290	0.222	0.262
	ResNet[Panda0.05]	0.897	0.726	0.724	0.706	0.446
	ResNet[Guassian+Panda]	0.770	0.104	0.122	0.184	0.134
	ResNet[Guassian+Panda] _T	0.838	0.092	0.107	0.244	0.173
SR	ResNet[Gaussian0.01]	0.774	0.366	0.928	0.206	0.110
	ResNet[Panda0.01]	0.915	0.040	0.212	0.724	0.880
	ResNet[Panda ColorDepth3]	0.898	0.078	0.288	0.582	0.438
	ResNet[Guassian+Panda]	0.819	0.086	0.348	0.250	0.138
	ResNet[Guassian+Panda] _T	0.805	0.318	0.836	0.220	0.136
NSR	AllConv	0.875	0.178	0.730	0.570	0.958
	AllConv[Guassian+Panda]	0.772	0.076	0.120	0.248	0.540
	AllConv[Guassian+Panda] _T	0.798	0.078	0.102	0.282	0.442



Figure 6: $\varphi_r(x)$, $\varphi_r(x')$ and differences results 1.

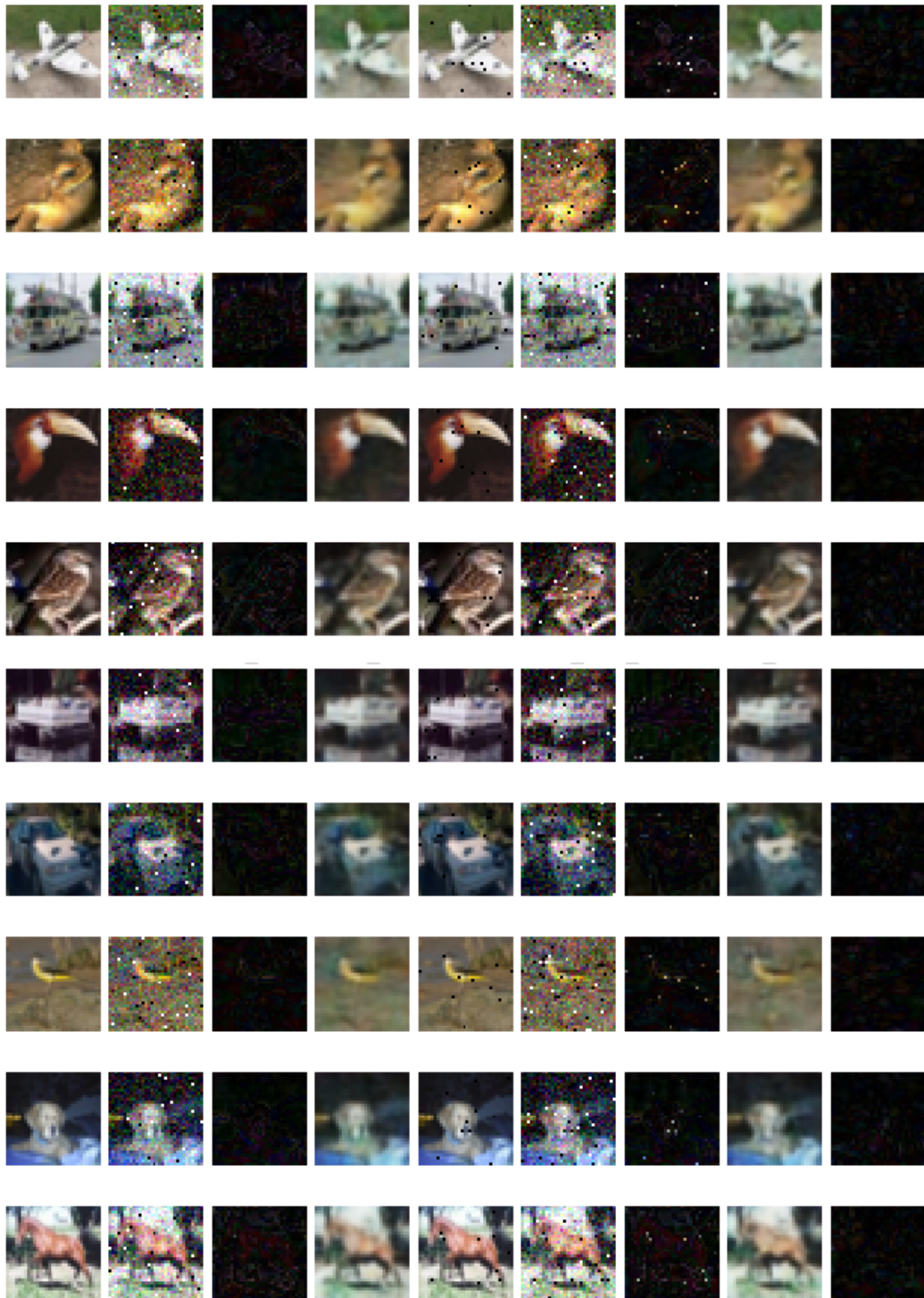


Figure 7: $\varphi_r(x)$, $\varphi_r(x')$ and differences results 2.

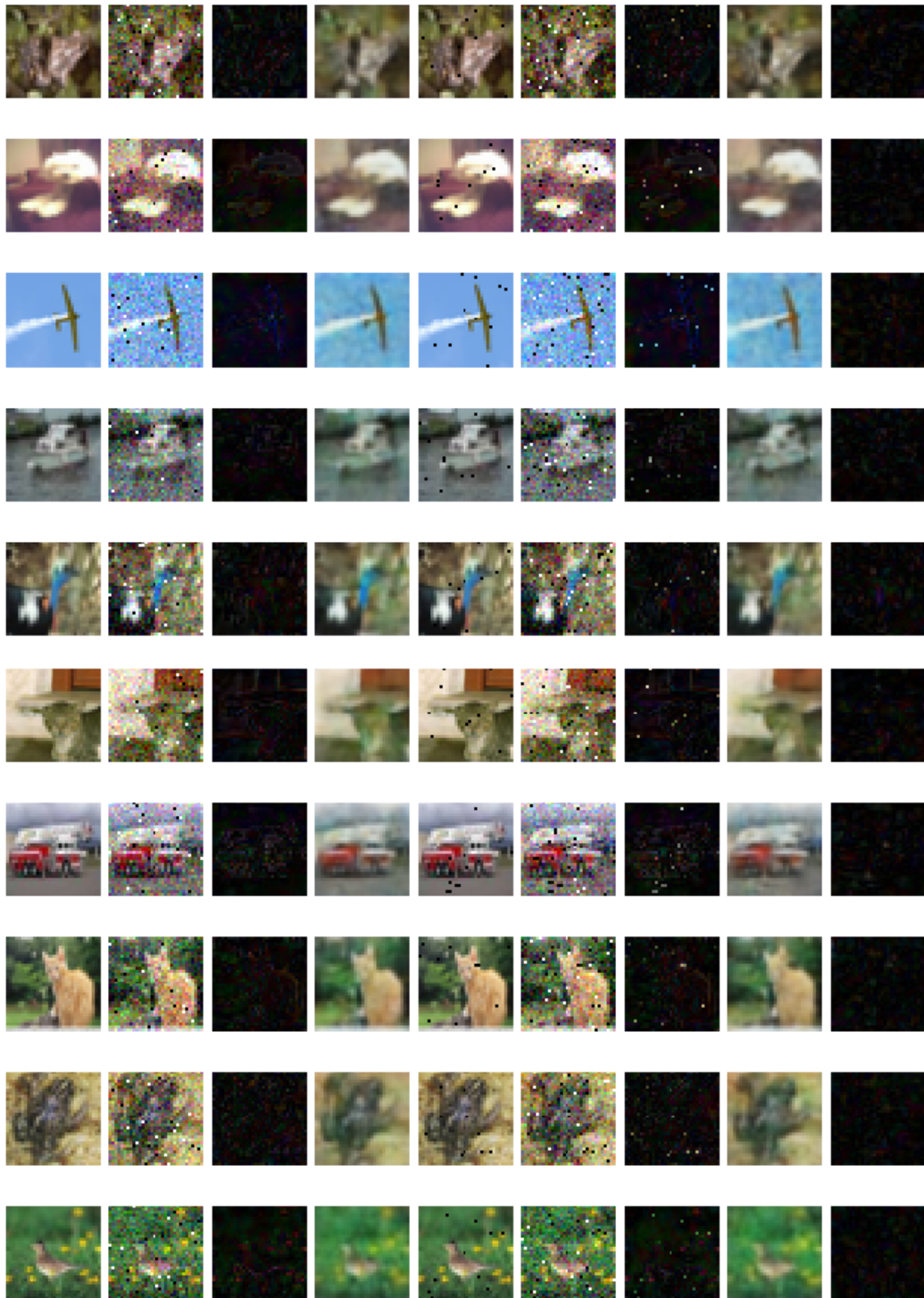


Figure 8: $\varphi_r(x)$, $\varphi_r(x')$ and differences results 3.

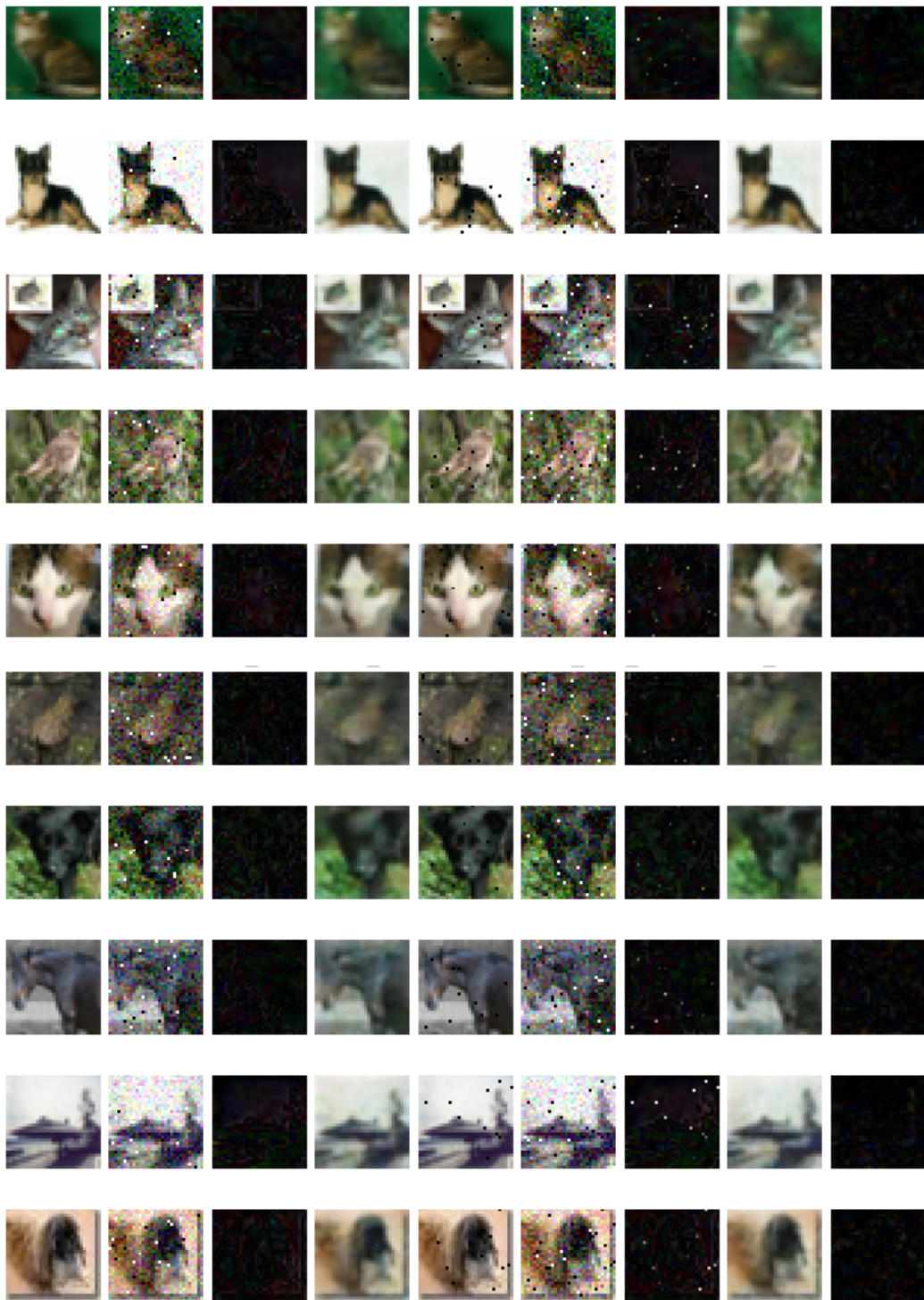


Figure 9: $\varphi_r(x)$, $\varphi_r(x')$ and differences results 4.

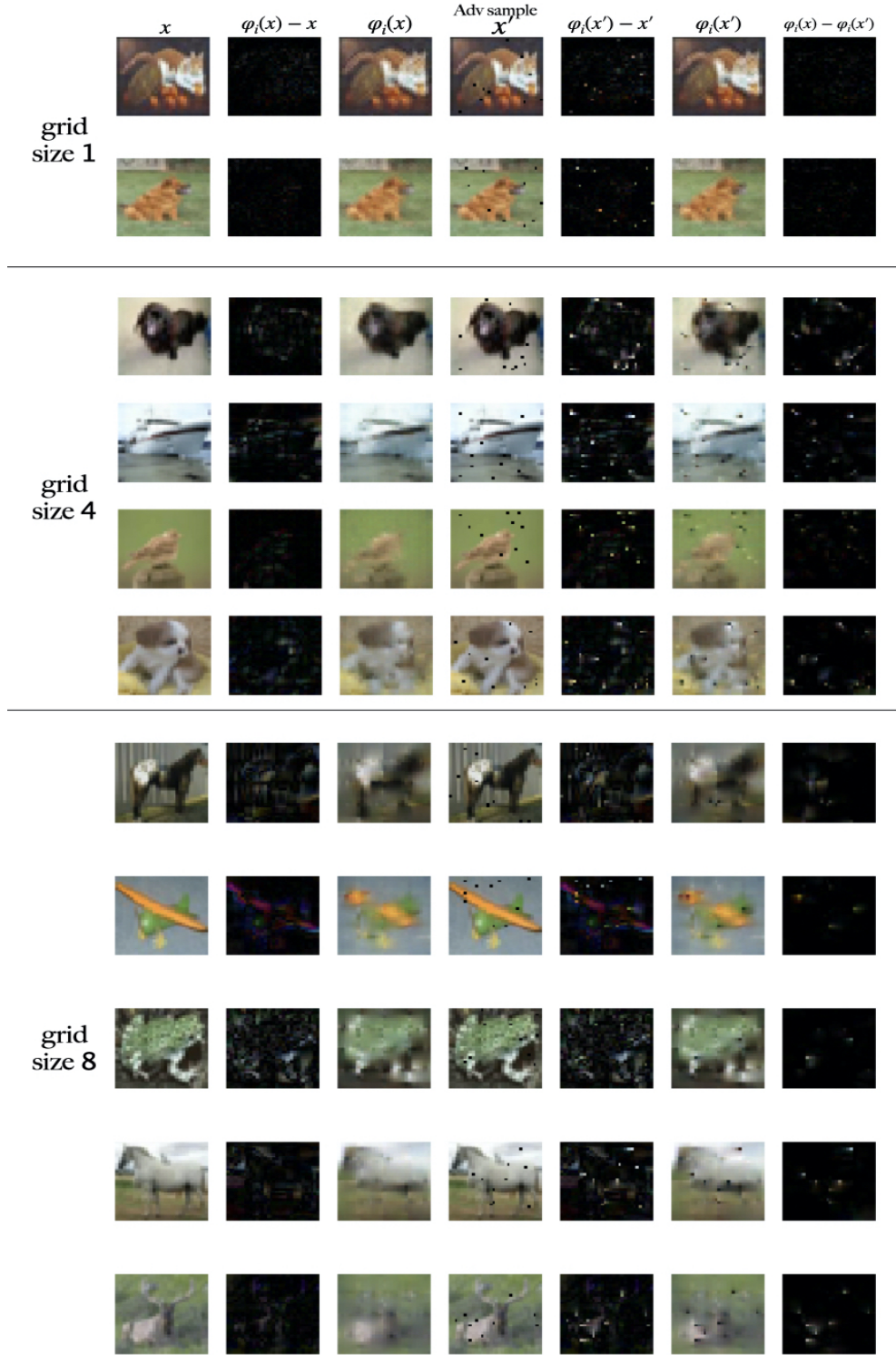


Figure 10: Example $\varphi_i(x)$ on an image x and its respective adversarial sample x' with Grid size 1, 4 and 8.